CARBON MANAGEMENT TECHNOLOGY CONFERENCE

CMTC-151748-PP

Improved Force Balance for Predicting Vertical Migration of CO_2 from Geologic Sequestration Sites

Shibo Wang and Andres Clarens
Department of Civil and Environmental Engineering, University of Virginia

Abstract

An improved model of CO_2 bubble rise through porous media in the deep subsurface is developed in an effort to better understand leakage processes under geologic carbon sequestration (GCS) conditions. Parcel of CO_2 will be subject to at least three dynamic forces: 1) buoyant forces; 2) surface tension forces; and 3) shear drag forces. To fully characterize these, this work involved several experimental measurements focused on the second and third forces in particular. To better understand the effect of shear drag forces, the viscosity of brines was explored under bubbly flow scenarios to understand the rheological conditions that might impact leakage. To better understand the role of surface tension forces on influencing flow, contact angle measurements were carried out for a range of relevant mineral, brine, CO_2 combinations. Predicting leakage from geologic carbon sequestration sites is difficult because of the large length scales that are involved and because of the complex geophysics and geochemistry that a rising parcel of CO_2 will be subject to as it travels to the surface. To better understand how quickly and where a parcel of CO_2 is likely to escape, better modeling tools are needed. These tools must be based on experimental results collected for GCS-relevant conditions. The results of the brine viscosity work suggest that under vapor liquid equilibrium (VLE) conditions CO_2-brine mixtures will exhibit complex viscoelastic behavior. This is because CO_2 bubbles in the matrix will respond to the varying levels of shear that will exist in the porous media to resist flow. Similarly, the contact angle measurements suggest that CO_2 is less wetting of some common minerals and clays that prevail near GCS sites. The experimental results described here will be used to describe an enhanced model of CO_2 vertical flow through the subsurface. The effects and relative importance of five modeling parameters including viscosity of endogenous brines, contact angle between CO_2 and formation minerals, CO_2 bubble size, particle size and pore size of porous media are evaluated. The results suggest that each of these parameters is important for controlling leakage and that the priority depends on the characteristics of the formation. At smaller scales, this enhanced model could help explain preferential flow pathways and potential hysteresis that could influence leakage from GCS sites. At larger scales, the results of this work could contribute to more accurate prediction tools for managing the risk associated with GCS.

Keywords: Geologic carbon sequestration, leakage/seepage, flow through porous media, bubble flow, contact angle.

Introduction

Geologic carbon sequestration (GCS) has been discussed as a scalable and economically viable approach for keeping large volumes of anthropogenic carbon dioxide out of the atmosphere (Chen, Gingras et al. 2003; Eccles, Pratson et al. 2009). In GCS, the flue gas from power plants and other point sources is captured, separated, compressed, transported and injected into porous geologic formations several kilometers under the surface. Candidate formations are bound by impermeable layers that prevent the buoyant rise of the injected CO_2 and are generally filled with brines that would have little other economic value (Widjajakusuma, Biswal et al. 1999; Kneafsey and Pruess 2010). At these depths, hydrostatic pressures and geothermal temperatures are large and the CO_2 exists in the liquid or supercritical phase where it would intermingle with the endogenous brines (Chen and Zhang 2010). The densities of CO_2 under all states are lower than that of the native brines and so the parcel of CO_2 will be subject to buoyant forces. The CO_2 could escape under several scenarios including leakage through abandoned well bores, heterogeneities in the bounding formation, groundwater flow to shallower unconfined aquifers and other pathways (Figure 1 (left)) (Nordbotten, Celia et al. 2004; Zhang, Oldenburg et al. 2009; Wollenweber, Alles et al. 2010).

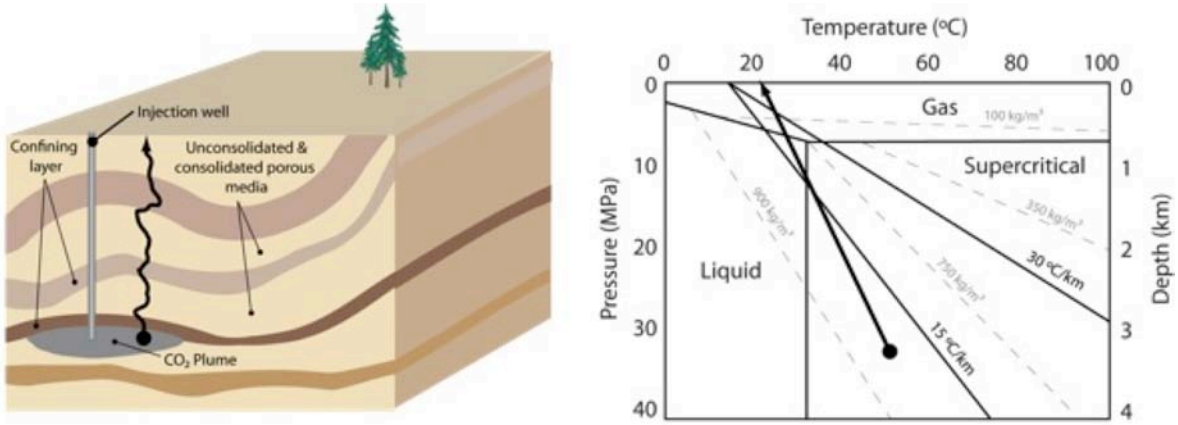

Figure 1. Leakage from geologic carbon sequestration sites will involve CO_2 vertical transport through numerous subsurface formations (left). The CO_2 will undergo at least one phase transition in its rise to the surface as a result of hydrostatic pressure and thermal gradients in the subsurface (right).

The benefits of GCS would be greatly diminished if appreciable amounts of CO_2 leaked to the atmosphere. Leakage would both represent a loss of carbon mitigation potential and it could also imply a net contribution to greenhouse gas (GHG) emissions because of the energy consumed in the failed CO_2 capture and storage operation (Pollak and Wilson 2009). Leakage may also have health, safety and environmental (HSE) consequences, such as contamination of potable water resources, or worse, dangerous displacement of air at the land surface (Birkholzer and Zhou 2009). Reported eruptions from naturally occurring reservoirs provide evidence for the possibility of CO_2 discharges from the sub-surface (Pruess 2008). At present, the uncertainty and risk associated with leakage processes is one of the most significant roadblocks to widespread implementation of the technology. Yet these processes are challenging to study on the field scale because of the extensive heterogeneity that exists at these sites and because cause-and-effect relationships are difficult to establish (Patzek, Silin et al. 2003; Oldenburg, Lewicki et al. 2010). In the lab, these processes are difficult to study because experiments of flow through porous media at high pressure do not easily scale down and the heterogeneities in the subsurface make it challenging to develop first-principles models of leakage under GCS conditions.

A few characteristics of this problem have been described in the literature (Oldenburg and Lewicki 2006). First, as CO_2 rises in response to the geothermal and hydrostatic pressure gradients that exist in the subsurface, phase separation and ebullition in supersaturated brines may occur as the pressure or temperature drops. The formation of discrete CO_2 bubbles would change phase from supercritical, possibly existing as a liquid and ultimately ending up as a gas near the surface (Figure 1 (right)). A rising parcel of CO_2 may accelerate due to the increased buoyancy that comes from expansion of CO_2 from supercritical (i.e., $CO_{2(sc)}$) to subcritical conditions (i.e., either $CO_{2(l)}$ or $CO_{2(g)}$) (Oldenburg 2007; Pruess 2008). In Figure 1, the dark black circles represent the CO_2 reservoirs. The salinity of the endogenous brine strongly affects the solubility of CO_2 and hence influences the leakage rate of CO_2. When the CO_2, exists in the supercritical or gas phase it will exist in vapor liquid equilibrium (VLE) with the endogenous brine. Depending on the rate of leakage, the leaking parcel of CO_2 might expand adiabatically resulting in Joule-Thomson cooling that could impact density difference and result in nonlinear vertical velocity profiles (Pruess 2008). The viscosity contrast between a rising parcel of CO_2 and the brine it is displacing makes it more likely that instabilities and fingering will occur (Riaz and Tchelepi 2008). The rate at which CO_2 leaks will impact secondary trapping processes such as capillary trapping, dissolution/precipitation reactions, and temperature effects (Li, Peters et al. 2006). To date, these issues have not been explored in a comprehensive manner.

The goal of this work is to develop an improved force balance on leaking parcels of CO_2 from GCS sites using a combination of improved experimental results and several modeling frameworks. Existing models of bubble rise and bubble rise through porous media are combined to consider the effects of temperature, depth (pressure), salinity, viscosity of the endogenous fluid, contact angle between CO_2 and formation minerals and degree of mixing. Existing work has largely assumed constant values for

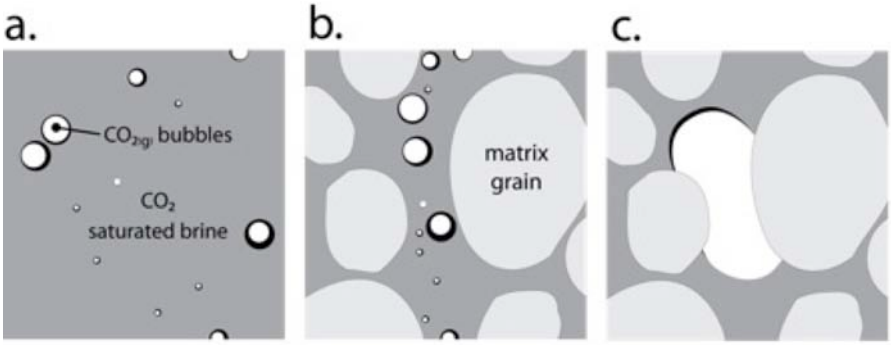

Figure 2. Buoyancy-driven CO_2 bubble rise regimes: a. CO_2 bubble free rise in CO_2-saturated brine b. small CO_2 bubble free rise through coarse porous media without contact with pore walls c. CO_2 channel flow through porous media

viscosity and contact angle and this work incorporates experimental data for both under GCS relevant conditions (Corapcioglu, Cihan et al. 2004). The work is organized into two parts, in the first, CO_2 bubble free rise in CO_2-saturated brine and small CO_2 bubble free rise through coarse porous media without contact with pore walls is considered (Figure 2a,b) and in the second, CO_2 channel flow through porous media is modeled (Figure 2c). The existing models of CO_2 transport under these conditions are validated to quantify the rise velocity of CO_2 in an otherwise brine-saturated porous media and to evaluate the relative importance of model parameters including viscosity of matrix fluid, contact angle between CO_2 and formation minerals, CO_2 bubble size, particle size and pore size of porous media with experimental data.

Experimental Methodology

Rheology of CO_2-brine mixtures

Viscosity of the interstitial bulk mixture of saline water in contact with $CO_2$was measured over a range of shear conditions. The viscosity of the CO_2-brine binary mixture has been reported in two publications but both have limitations (Kumagai and Yokoyama 1999; Bando, Takemura et al. 2004). In one study the viscosity was reported only at pressures higher than 100 bar (10 MPa). Many leakage processes will occur in shallower aquifers with hydrostatic pressure below 100 bar. The other study was limited because it measured viscosity under very low shear rate conditions. The effective shear forces experienced by fluids in geologic formations can be very high because of small pore diameters relative to the fluid flow velocity. Under these conditions, complex rheology could ensue that would impact CO_2 vertical transport. In this work, mixture viscosity was characterized over a range of relevant pressure, temperature, and ionic strength conditions. The viscosity of these mixtures was measured using an Anton-Paar MCR 301 rheometer equipped with a high-pressure measuring cell rated up to 150 bar (15 MPa). The CO_2 was delivered using a Teledyne ISCO 500HP syringe pump with a constant temperature jacket. A temperature jacket was needed to ensure that liquid CO_2 was delivered to the pressure cell at a known temperature. Temperature in the rheometer was controlled to within ± 0.1ºC using a peltier style temperature controller integrated into the rheometer. More details about this experimental setup can be found in (Wang and Clarens 2011).

Contact angle measurements

The three-phase contact angle between CO_2, brine, and the solid mineral surface were measured using a specially designed high-pressure cell. The cell contains a stage on which to mount a mineral sample, an injection port through which to add carefully measured volumes of CO_2, a high pressure pump for the brine, temperature and pressure controls, and two sapphire windows used to photograph the droplet. The contact angle is measured directly from the photographs using image processing software and axisymmetric drop shape analysis. The entire testbed is mounted on a stability table to permit for long-term (weeks) studies of the hysteresis of CO_2 on different mineral samples. In principle, this method of static drops is effective for predicting how well CO_2 advance through different porous media but very limited data exists for most of the mineral types that would be encountered in the subsurface.

Modeling Approach

In a broad sense, leakage processes of interest for GCS applications involve all those in which CO_2 escapes from the reservoirs into which it is originally injected. To understand these pathways, which are poorly described in the literature, it is first useful to consider the mechanisms by which CO_2 could become trapped in the subsurface. These trapping processes have been much better studied. After injection, supercritical/liquid CO_2 will stay on top of endogenous brine as a discrete phase due to buoyancy and it will be trapped underneath the caprock. This is known as structural trapping and will prevent immediate buoyant rise of the CO_2 while the slower trapping mechanisms commence. CO_2 will dissolve into brine and reach equilibrium that is a function of pressure and temperature. Precipitation of the dissolved carbonate materials with cationionc species in the formation brines will constitute permanent mineral trapping. Similarly, when the CO_2 reaches dead end pore spaces in the porous media, capillary trapping will occur that can persist over long length scales (Bachu 2008; Mansoori, Iglauer et al. 2009).

In cases where these permanent or semi-permanent trapping conditions do not exist, CO_2 or CO_2-saturated brines can rise through the subsurface in response to buoyant forces. For the CO_2-saturated brines the CO_2 will move via advection, diffusion and dispersion. As it moves to lower pressure and temperature formations closer to the surface, the CO_2 will become increasingly insoluble and this lead to the ebullition of CO_2 bubbles. The pressure within the bubble, described by Henry's Law (Crandell, Ellis et al. 2010) must exceed the sum of the hydrostatic pressure and the surface tension of brine which must be overcome to form the bubble, which can be expressed as:

$$P = \sum_i C_i H_i > P_y + P_{st} \qquad \text{Equation 1}$$

where the pressure inside the bubble P is equal to the sum of the partial pressures of the volatile species, C_i is the aqueous concentration of the volatile species i, H_i is the Henry's law coefficients for each species i, P_y is the hydrostatic pressure at depth y, and P_{st} is the surface tension pressure. Once a bubble exists it will rise in response to buoyant forces and its velocity can be determined whether or not it is in contact with the pore walls.

CO_2 bubble rise

Gas-phase CO_2 experience free rise when small bubbles, <1mm, rise upwards without contacting the wall of the pores, i.e. $\left(\mathrm{R}_{\mathrm{CO}_2} < \mathrm{R}_{\mathrm{P}}\right)$. For this simple case, the rise is driven by buoyancy force and retarded solely by drag force. Under low Reynolds's number conditions, the rise velocity of CO_2 can be described by Stokes Law, shown in Equation 2 (Poletto and Joseph. 1995). Low Reynolds number are generally those on the order of one, e.g, $R_e = \frac{\rho_{matrix} u \mathrm{d}_{\mathrm{CO}_2}}{\mu_{matrix}} \sim 1$, and this typically occurs when the CO_2 bubble diameter is less than 1mm. The size of the bubble is also important because small bubbles can be treated as rigid bodies, i.e., there is no deformation and the bubbles have a spherical geometry (McGinnis, Greinert et al. 2006).

$$u = \frac{\mathrm{d}_{\mathrm{CO}_2}{}^2 g(\rho_{matrix} - \rho_{CO_2})}{\gamma \mu_{matrix}} \qquad \text{Equation 2}$$

Where γ is a viscosity coefficient, expressed as $\gamma = 12\frac{\mu_{matrix}+1.5\mu_{CO_2}}{\mu_{matrix}+\mu_{CO_2}}$. Since $\mu_{matrix} \gg \mu_{CO_2}$, $\gamma = 12$. Viscosity is one of the most important thermophysical properties associated with CO_2 bubble rise since it directly impacts the drag force. Existing work has largely relied on the viscosity of pure water to approximate the characteristics of CO_2-saturated brine (Oldenburg and Lewicki 2006). To improve accuracy of calculation of CO_2 rise velocity by Stokes Law, condition specific viscosity from experimental measurements need to be used. Viscosity of CO_2-brine mixtures under a variety of temperature, pressure and salinity conditions were collected and included in the model.

CO_2 channel flow through porous media

Stokes law is useful for cases in which the bubble does not contact the walls of pores through which it is moving. Most of the CO_2 in a leaking parcel will contact the pore walls effectively creating channel flow conditions. For this case of buoyancy-driven channel flow of gases through flooded porous media, other models will be needed, and several have been proposed and explored in the literature. The modeling framework used here is based on the work Corapcioglu et al. who derived a theoretical model to describe the rise of air through a porous medium based on a macroscopic force balance acting CO_2 (Corapcioglu, Cihan et al. 2004). The model is based on several important assumptions: first, both the brine and the CO_2 are treated as incompressible. For the case of GCS, this is not always a reasonable assumption but Corapciouglu has proposed alternate solutions to his framework that would allow us to consider this situation (Cihan and Corapcioglu 2008). A second assumption is that the endogenous brine is saturated with CO_2 such that mass transfer between the bubble and the bulk is not considered. This means that diffusion and dispersion of CO_2 into the brine is neglected (Oldenburg and Lewicki 2006). A third assumption is that CO_2 reaches equilibrium with respect to temperature and pressure instantaneously. In practice, thermal gradients in the subsurface are subtle enough that this assumption is probably reasonable. A fourth assumption, which enables modeling at larger scales, is that the porous media is isotropic and fully saturated with brine before CO_2 penetration. Again here, this assumption is unlikely in the real world but it does greatly simplify the calculations. A fifth assumption is that there is no bubble generation mechanisms such as snap-off and division, which would occur in dead-end pores and other places in the formation where the channel could not continue. Under steady state leakage conditions, this is probably a reasonable assumption. The sixth assumption is that there is no Basset history force that results from the viscous effects generated by the acceleration of a particle relative to a fluid under the creeping flow conditions (Zhang and Fan 2003). Seventh, the lift force acting on a bubble is neglected because of irrotational flow conditions (Soubiran and Sherwood 2000). Eighth, the fluid flow in the endogenous brine around a rising bubble and within the fluid bubble is neglected. Finally, velocity gradients are only considered in the vertical direction.

When these assumptions are met, a force balance on a rising bubble in contact with the pore walls forms the basis for an analytical model of channel flow (Ergun 1952). The governing equation incorporates inertial force, added mass force, buoyant force, surface tension and drag force that results from the momentum transfer between different phases. As shown in Figure 3, buoyancy force $F_b$provides the fundamental driving force for CO_2 to rise, and surface tension F_{st} and drag forces F_d resist the motion. The added mass force F_A originates from the acceleration of discrete CO_2 mass relative to the matrix fluid in the perturbed flow field (Wallis 1969). Considering the spatial and transient nature of the rise velocity, linear momentum of CO_2 rising in an otherwise brine saturated porous media is conserved following Equation 3.

$$\sum F = \frac{D}{Dt}\left(\rho_{CO_2} v u\right) = F_A + F_b + F_d + F_{st} = \left(\rho_{CO_2} + C_M \rho_{matrix}\right) V \left(\frac{\partial u}{\partial t} + u\frac{\partial u}{\partial y}\right)$$

Equation 3

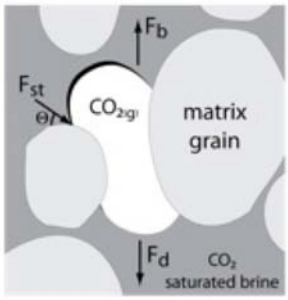

Figure 3. Forces applied on CO_2 channel flow through porous media.

The added mass term is defined as:

$$F_A = \frac{D}{Dt}(C_M \rho_{matrix} V u) \quad \text{Equation 4}$$

where C_M is the added mass coefficient which depends on the geometry of the CO_2 bubble, ρ_{matrix} is the density of the matrix fluid, V is the volume of CO_2 bubble, u is the rise velocity of CO_2.

The buoyancy force is defined as:

$$F_b = (\rho_{matrix} - \rho_{CO_2}) g V \quad \text{Equation 5}$$

where ρ_{CO_2} is the density of CO_2 and g is the acceleration of gravity. The surface tension force is:

$$F_{st} = 2\pi R_p \sigma \sin\theta \quad \text{Equation 6}$$

where R_p is the equivalent radius of a pore throat through which CO_2 can pass in a particular arrangement of sedimentary particles, σ is the surface tension at CO_2-brine interface and can be described with Young-Laplace equation, θ is the equilibrium contact angle of CO_2 contacting the wall of the pores. And the drag force on the parcel of CO_2 is defined as:

$$F_d = AV\left[\left(\frac{150\mu_{CO_2} u(1-\phi)^2}{d_p^2 \phi^3} + \frac{1.75\rho_{CO_2} u^2 (1-\phi)}{d_p \phi^3}\right)\right] \quad \text{Equation 7}$$

where A is the correction factor incorporating the effects of media-specific properties and contact pattern of CO_2 with pore materials such as tortuosity, the shape factor and surface area (Cihan and Corapcioglu 2008), μ_{CO_2} is the dynamic viscosity of CO_2, ϕ is the effective porosity of the porous media, and d_p is the mean diameter of the sedimentary particles.

The drag term in this force balance is the most difficult to quantify because the momentum transfer caused by drag force is impacted by heterogeneities in the pore geometry. Recognizing that drag force is associated with both kinetic and viscous energy losses, semi-empirical solutions to this term have been prepared such as those reported in the modified Ergun equation (Ergun 1952). This approach is adopted here. The viscous energy losses are accounted by the Kozeny equation for laminar flow and the kinetic energy losses are described by Burke-Plummer equation for turbulent flow (Corapcioglu, Cihan et al. 2004). This theoretical methodology has been validated with experimental data reported in the literature including cases that are relevant to GCS case (Roosevelt and Corapcioglu 1998). After making one additional substitution for the volume of CO_2 (i.e., $V = \frac{4}{3}\pi {R_{CO_2}}^3$ where R_{CO_2} is the equivalent radius of a sphere with a volume equal to that of a specified bubble) the conservation of momentum equation can be written as:

$$\frac{4}{3}\pi {R_{CO_2}}^3 g(\rho_{matrix} - \rho_{CO_2}) - \frac{4}{3}\pi {R_{CO_2}}^3 A\left[\left(\frac{150\mu_{CO_2} u(1-\phi)^2}{d_p^2 \phi^3} + \frac{1.75\rho_{CO_2} u^2(1-\phi)}{d_p \phi^3}\right)\right] - 2\pi R_p \sigma \sin\theta$$
$$= \frac{4}{3}\pi {R_{CO_2}}^3 (\rho_{CO_2} + C_M \rho_{matrix})\left(\frac{\partial u}{\partial t} + u\frac{\partial u}{\partial y}\right) \quad \text{Equation 8}$$

The solution to this equation under steady state conditions (i.e., $\frac{Du}{Dt} = 0, C_M = 0$) is the terminal velocity of CO_2 bubble rise under channel flow conditions and it can be written as follows (Corapcioglu, Cihan et al. 2004):

$$u = \frac{\mu_{CO_2}(1-\phi)}{\rho_{CO_2} d_p}\left[-42.86 + \sqrt{1836.74 - \frac{0.57}{A}\left(\frac{\rho_{CO_2} d_p^3 \phi^3}{{\mu_{CO_2}}^2 (1-\phi)^3}\right)\left(\frac{1.5 R_p \sigma \sin\theta}{{R_{CO_2}}^3} - (\rho_{matrix} - \rho_{CO_2}) g\right)}\right] \quad \text{Equation 9}$$

Conditions considered here

To describe leakage processes over a range of relevant conditions, two P-T paths were chosen as the basis for the experiments and simulations reported here (Table 1). The first represents near surface conditions whereby CO_2 would begin at 40°C and 4MPa and then rise to a point where the conditions are at 30°C and 1MPa. This first condition corresponds to an average surface temperature of 26°C and a linear thermal gradient of 33.3 °C/km. The second would be representative of a more significant leakage event with the CO_2 originating under conditions corresponding to deeper formations, 50°C and 20MPa, and subsequently rising to a shallower formation with conditions of 30°C and 7MPa. This corresponds to a surface temperature of 19°C and a linear thermal gradient of 15.4 °C/km.

Table 1. Leakage paths investigated in this study

Leakage Path	Temperature (°C)	Pressure (MPa)	Depth (km)	Phase State	Surface Temperature (°C)	Thermal Gradient (°C/km)
1	30	1	0.1	Gas	26.7	33.3
	40	4	0.4	Gas		
2	30	7	0.7	Gas	19.2	15.4
	50	20	2	Supercritical		

To improve on existing frameworks for evaluating bubble rise through porous media, a detailed sensitivity analysis was carried out on the Corapcioglu model and an improved F_{st} term was used based on updated contact angle results collected in our laboratory. The sensitivity analysis was carried out to evaluate the relative importance of five key model inputs, namely the effective porosity ϕ, grain size d_p, contact angle between CO_2 and mineral surfaces θ, bubble size R_{CO_2} and pore size R_p on affecting the rise velocity of CO_2. The two cases described in Table 1 (e.g., P-T conditions corresponding to 30 °C and 7MPa, 50 °C and 20MPa) are investigated. The corresponding thermophysical property parameters used are listed in Table 2. For the five experimental inputs of interest, statistical ranges were defined and these are presented in Table 3. The values for Case 1 were selected to approximate the properties of Berea sandstone and the values for Case 2 were selected to represent particles of relatively uniform and larger grain size packed in the pattern of orthorhombic arrangement (as in (Corapcioglu, Cihan et al. 2004)). The Berea sandstone case represents the scenario of relatively small porosity, pore size, matrix grain size and bubble radius while Case 2 bounds the conditions at the other end. A few different types of distribution for these five variables including normal, log-normal, gamma and Weibull were tested to fit the data and the results indicate that log-normal generally has a superior fit to all the variables. The statistical characteristics are regressed with respect to lognormal distribution using Microsoft® Excel "Solver" add-in. A Monte-Carlo analysis on the stochastic sensitivity of respective variables were carried out using these distributions of parameters as model inputs using the Oracle® Crystal ball.

Table 2. Model parameter used in this work

Parameters	Units	Values		References
gravitational acceleration, g	m/S2	9.81		
density of brine, ρ_{matrix}	kg/m3	1020		
Correction factor, A		26.8		(Corapcioglu, Cihan et al. 2004)
Surface tension, σ	N·m	0.04		(Chiquet, Daridon et al. 2007; Espinoza and Santamarina 2010)
		Low	High	
Temperature, T	oC	30	50	
Pressure, P	MPa	7	20	
Depth	m	700	2000	
Ionic Strength, S	mol/L	7.1~7.6x10^{-4}	0.65	
viscosity of CO_2, μ_{CO_2}	Pa·S	2.14E-05	6.87E-05	(Wang and Clarens 2011)
density of CO_2, ρ_{CO_2}	kg/m3	266.56	784.29	(Span, Lemmon et al. 2000)

Table 3. Model parameters used in Oracle® Crystal Ball. All parameters are fit to lognormal distributions.

	Case 1		Case 2		
Parameter	$\bar{x}$	σ	$\bar{x}$	σ	Reference
Effective Porosity (%)	0.2386	0.056	0.3954	0.2	(Widjajakusuma, Biswal et al. 1999; Song 2001; Chen, Gingras et al. 2003; Padhy, Lemaire et al. 2007)
Grain Size (m)	0.00025	0.00008	0.004	0.003	(Peters 2009; Glover and Walker 2011)
Pore Throat (m)	0.00001	0.00000254	0.0001	0.00005	(Song 2001; Padhy, Lemaire et al. 2007)
Bubble Radius (m)	0.0005	0.0003	0.002	0.001	Preliminary experimental data

Results

CO_2 bubble rise

Dissolved CO_2 has been shown to increase the viscosity of brines and this behavior is consistent with other acidic solutions that exhibit higher viscosity than water alone (Bando, Takemura et al. 2004). The magnitude of this viscosity increase is typically small (<20%). A much more significant increase in the effective viscosity of the solution was observed after phase separation when the presence of bubbles increased the shear drag force. Bubbles resist deformation and this effect can increase the viscosity of the brine by 300-400%. At higher temperatures and higher ionic strength, the effect is less pronounced. The full results are reported in Wang 2011 (Wang and Clarens 2011). Select data from this research and additional results are presented in Table 4.

Table 4. Experimental data of viscosity (mPa·s) used in Stokes Law

		Vapor-Liquid Equilibrium (VLE)		Liquid-Liquid Equilibrium (LLE)	
		Ionic strength of brine (M)			
Temperature (°C)	Pressure (MPa)	3.1-7.6×10^{-4}	0.53	3.1-7.6×10^{-4}	0.53
30	1	1.43~5.39	0.98~4.14	0.84	0.85
	4	2.37~5.42	1.98~5.37	0.86	0.88
40	1	0.85~3.85	0.96~3.63	0.65	0.66
	4	1.85~4.18	1.66~4.46	0.67	0.69

The fluid viscosity μ_{matrix} results reported in Table 4 were then used as input to the Stokes law and the results are shown in Figure 4a as a function of bubble diameter d_{CO_2}. The viscosity of the brine has an important effect on controlling terminal rise velocity over a range of bubble sizes even though the effect is most pronounced for larger bubbles. This result, while obvious given the mathematical form of the Stokes law in Equation 2, is worth consideration in light of the new viscosity data presented in Table 4. Once bubble ebullition commences, terminal velocity could drop by more than 75% over a range of relevant bubble sizes. Expressed as a function of the brine viscosity, CO_2 bubble rise velocity drops according to the quadratic proportionality in the Stokes law. The impact of viscosity was evaluated for four bubble sizes, 0.000075, 0.00015, 0.0005 and 0.00075m and the results are shown in Figure 4b. Larger bubbles have a higher terminal velocity, e.g., the terminal velocity of a 0.00075m bubble is 100 times of that of 0.000075m bubble. The effect of viscosity on terminal velocity depends on the ratio $\frac{(\Delta d_{CO_2})^2}{\Delta \mu_{matrix}}$. As a CO_2 bubble follows the P-T path described in pathway 1 in Table 1, it will have a rise velocity in the range of 0.00085 to 0.643 m/s depending on the salinity of the endogenous brine. These swings in rise velocity over many orders of magnitude are significant for beginning to bound the uncertainty associated with estimates of CO_2 leakage from GCS sites.

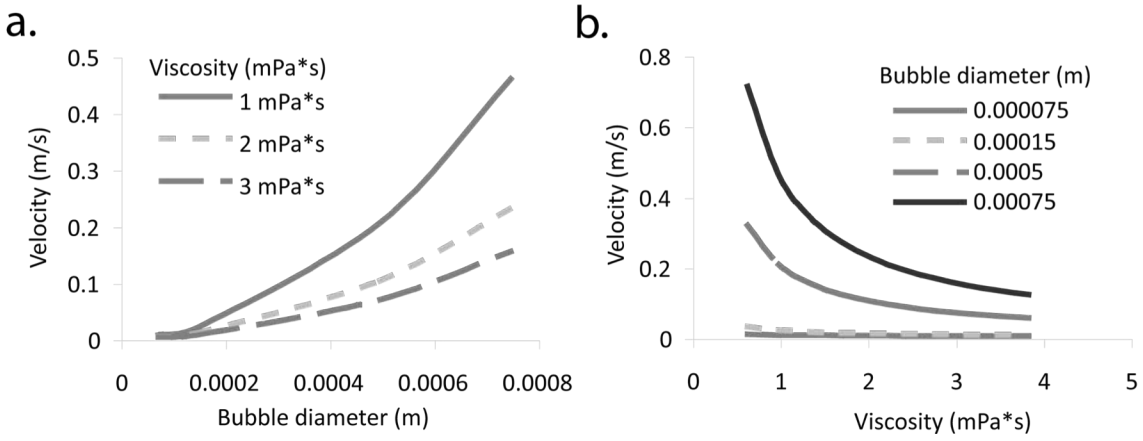

Figure 4. Effect of (a) bubble size and (b) viscosity on buoyant driven rise of CO_2 through brines under GCS relevant conditions.

CO_2 free rise through porous media

Most models of bubble rise through porous media have assumed a constant value for contact angle (150°) (Oldenburg and Lewicki 2006; Cihan and Corapcioglu 2008). In reality this value varies as a function of the composition of the host formation. Peters reported that even though digenetic clay minerals such as Kaolinite may only account for 5% to 31% of the formation by mass, they account for much more of the pore-mineral contact boundaries, typically in the range of 65% to 86% (Peters 2009). This suggests that more detailed data on interfacial properties are needed for developing accurate models of bubble rise. This same study found that kaolin is responsible for 75% of pore-mineral contact boundaries, quartz for 17%, feldspar for 5% and calcite for 3%. Contact angle measurements for the solids were carried out here and the results are presented in Table 5. An effective contact angle term is defined that is a weighted average of the contact angles and the percentage distributions measured by Peters. The distribution characteristic numbers are regressed and summarized in Table 6.

Table 5. Results of contact angle measured in this work

Mineral	Temperature (°C)	Pressure (MPa)	Ionic Strength (M)	
			7.1~7.6x10^{-4}M	0.65M
			Contact angle (°)	
Kaolin	30	7	158.16	155.92
	50	20	161.26	154.5
Quartz	30	7	151.26	154.75
	50	20	152.48	156.5
Feldspar	30	7	150.86	161.66
	50	20	161.06	160.36
Calcite	30	7	143.06	151.01
	50	20	151.21	146.55

Table 6. Statistical distribution of contact angle

Experimental Conditions				Log-Normal Distribution	
Temperature (°C)	Pressure (MPa)	Depth (m)	Ionic Strength (M)	Mean	Standard Deviation
30	7	700	7.1~7.6x10^{-4}M	156.17	13.39
30	7	700	0.65M	155.86	19.48
50	20	2000	7.1~7.6x10^{-4}M	159.46	23.74
50	20	2000	0.65M	154.89	17.85

Using the two groups of distribution characteristics (Case 1 and 2) for impact factors presented in Table 1 and the measured contact angle data, the CO_2 rise velocity through porous media was estimated (Table 7). These modeling results demonstrate the important effect that formation characteristics can have on bubble rise velocity with the CO_2 rising through the Case 2 formation moving much faster than through the Case 1 formation. The full distributions of the bubble rise velocity as estimated using crystal ball are shown in Figure 5. As expected, the velocity of the bubble increases near the surface. Given how much slower the CO_2 leaks from deep formations, it strongly supports efforts to put CO_2 into the deepest formations that are economically viable. Using the mean linear velocities estimated here, assuming that velocity would increase according to a linear interpolation, and that a parcel of CO_2 was not trapped (e.g., it had an unobstructed hydraulic path to the surface), a formation described in Case 1 would leak in 240 days while a formation described by Case 2 would leak in 1.35 days.

Table 7. Distribution of rise velocity of CO_2 bubble flow

Experimental Conditions				Rise Velocity Distribution (m/s)	
Temperature (°C)	Pressure (MPa)	Depth (m)	Case	Mean	Standard Deviation
30	7	700	1	0.000085	0.00081
			2	0.0175	0.0413
50	20	2000	1	0.00004	0.00049
			2	0.0048	0.011

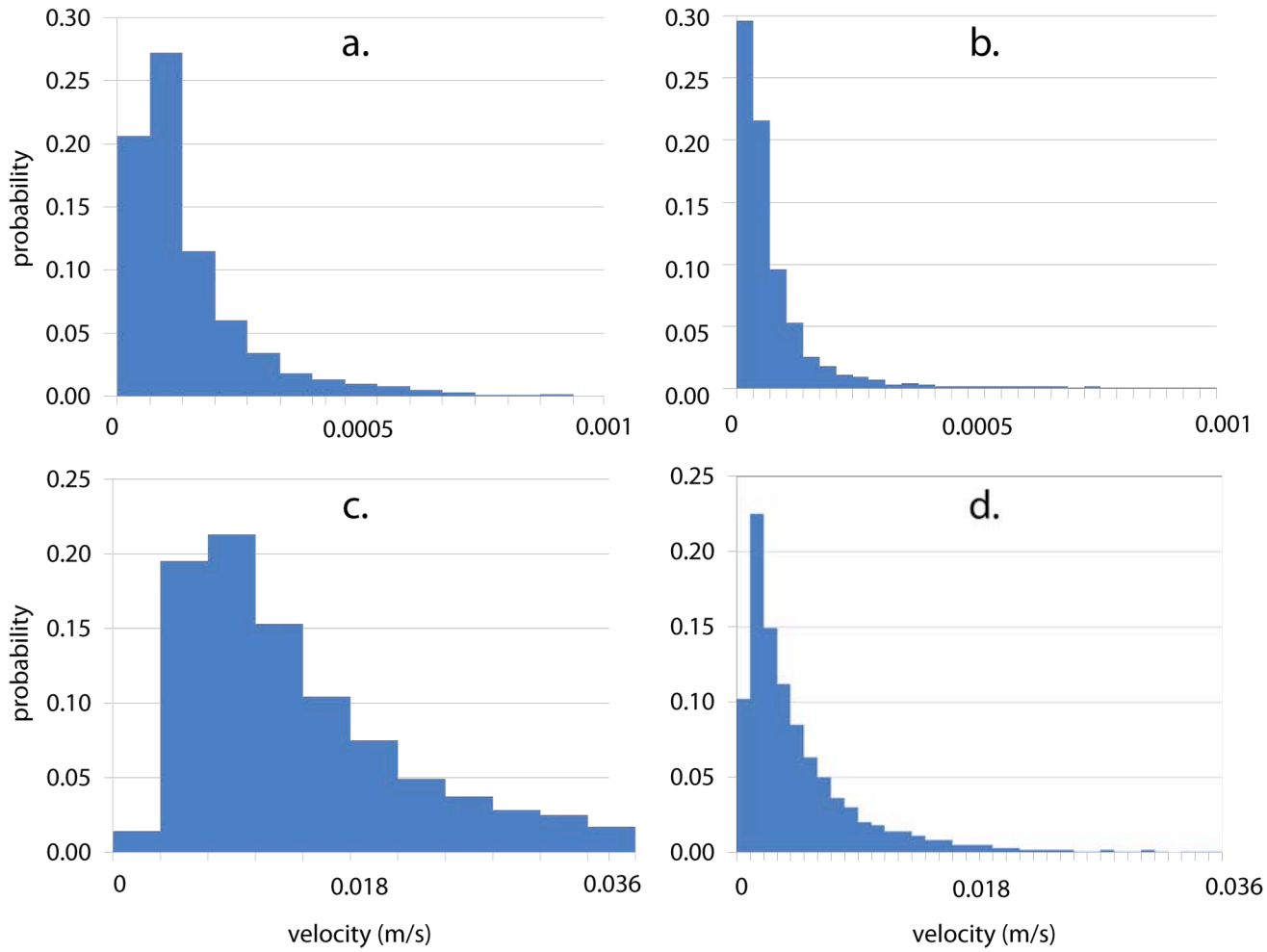

Figure 5. Distributions of bubble rise velocity estimate. Case 1: (a) 30ºC, 7 MPa; (b) 50ºC, 20 MPa; Case 2: (c) 30ºC, 7 MPa; (d) 50ºC, 20 MPa.

The sensitivity of the bubble rise through porous media model was assessed and the results are shown in Figure 6. These tornado plots illustrate the top 5 input parameters (contact angle, CO_2 bubble radius, effective porosity, grain size and pore size of porous media) to impact the velocity estimates of the model. These are calculated by varying each input parameter in turn via a ±10% change in the magnitude of the parameters. The centerline in these plots represents the baseline case as reported in Table 7. The light and dark-shaded bars imply direct or inverse relationships, respectively. In other words, velocity is positively correlated with some variables (contact angle, CO_2 bubble radius, effective porosity and grain size) and negatively correlated with others (pore throat). The results in Figure 6a correspond to the Case 1 condition (i.e., porous media with smaller effective porosity, grain and pore sizes and CO_2 bubble radius). Under these conditions, contact angle has the highest impact on the terminal rise velocity of CO_2, followed by CO_2 bubble radius, effective porosity, grain size and pore size of porous media. To illustrate how big of an effect contact angle is under these conditions, it is useful to consider that a 10% increase in contact angle results in an increase from 1.66×10^{-5} to 7.98×10^{-5} m/s in CO_2 rise velocity (a 400% increase). Meanwhile, a 10% increase in pore throat results in a decrease from 5.18×10^{-5} to 4.06×10^{-5} m/s in CO_2 rise velocity (a 22% decrease). For equivalent formation conditions, the importance of these model inputs seems to remain constant. The results under Case 2 conditions (Figure 6b), which represents the scenario of relatively large values of effective porosity, grain and pore sizes and CO_2 bubble radius, the sensitivity is somewhat different with effective porosity being most important followed by grain size, contact angle, bubble radius and pore throat. These results are consistent with more anecdotal observations of related systems. For example, Corapcioglu observed that surface tension forces, which are directly proportional to contact angle have the most significant effect on smaller bubbles (Corapcioglu, Cihan et al. 2004).

The effect of wetting vs. nonwetting behavior on mineral surfaces was considered in the context of the sensitivity analysis. Because of the sinusoidal function that includes contact angle, the net effect on vertical bubble velocity is the same for wetting and nonwetting surfaces (because $\sin\theta = \sin(\pi - \theta)$). When contact angles are complementary, nonwettability, i.e. large contact angle is much more favorable than wettability because the capillary pressure resulting from larger contact

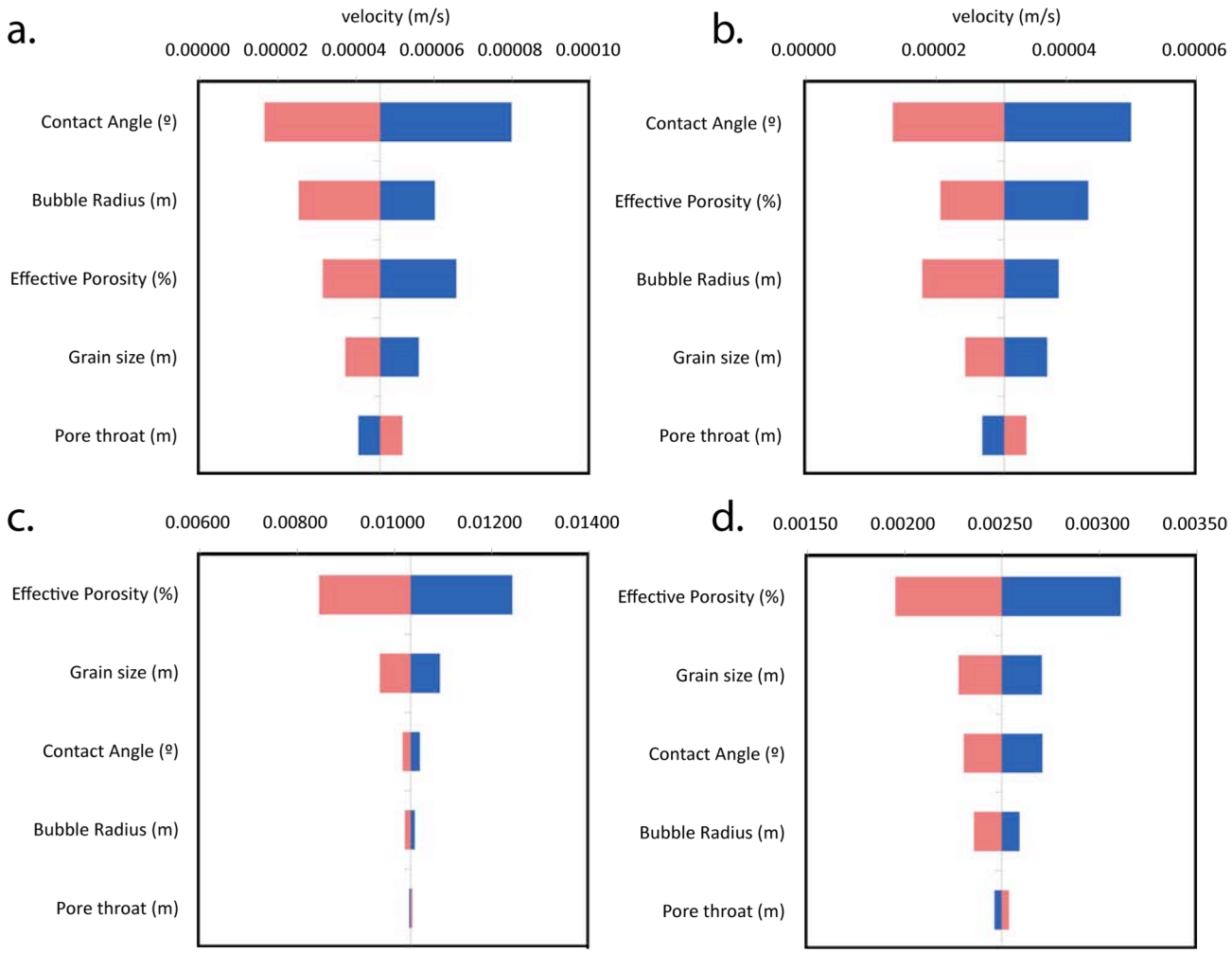

Figure 6. Tornado plots manifest to what extent CO_2 rise velocity is sensitive to a ±10% change in input parameters including contact angle, CO_2 bubble radius, effective porosity, grain size and pore size of porous media. Case 1: (a) 30ºC, 7 MPa; (b) 50ºC, 20 MPa; Case 2: (c) 30ºC, 7 MPa; (d) 50ºC, 20 MPa.

angles could have greater capacity for capillary trapping thereby providing the time for other, permanent sequestration processes to occur such as mineralization or dissolution (Chiquet, Daridon et al. 2007).

Discussion and conclusion

Before geologic carbon sequestration can be widely deployed, it is imperative that leakage processes be better characterized. This work combined experimental results with applicable modeling frameworks to provide a first look at how parcels of CO_2 would travel over long distances. The models are based on Stokes law and Ergun's equation for buoyancy driven flow of gas through porous media. Experimental data including detailed viscosity measurements and contact angle measurement allowed for more detailed analysis of the interfacial properties of this problem than had been reported in the past. Quantitative sensitivity analysis were performed to understand which parameters have the greatest impact on the bubble rise velocity and the ranking was found to change depending on the characteristics of the host formation.

Despite the advances reported here, this work only begins to describe the behavior of CO_2 vertical transport in the subsurface. There are several simplifying assumptions made here that should be explored in further detail including the assumption that the fluids in this problem are incompressible. Gas density vary with pressure and the nonzero flux on the surface results in a ''slip flow". There is also the possibility that hysteretic pathways will form through which surface chemistries are altered, e.g., low-pH brine would react with aluminosilicate or carbonates to expose different formations underneath. Mass transfer between CO_2 bubbles and surrounding brine could further complicate the process. Finally, instability such as viscous figuring created in the heterogeneous porous media will certainly impact the assumptions made here about vertical flow. By combining experimental and modeling techniques, each of these factors can be described so that leakage from GCS sites can be anticipated and prevented.

Acknowledgement
The authors thank Brian Tison, Ian Edwards, Sara Persily and Bo Liang for their assistance in data collection. This work was funded by the National Science Foundation (CBET-1134397).

Nomenclature

X_{CS} – CO_2 solubility under a specific temperature and pressure condition
P – Pressure, MPa
T – Temperature, ^oC
t – Time, S
S – Salinity, mass fraction of NaCl, %
g – Gravitational acceleration, m/S^2
u – Rise velocity of CO_2, m/S
d_{CO_2} – Diameter of CO_2 bubble, m
ρ_{matrix} – Density of brine, kg/m^3
ρ_{CO_2} – Density of CO_2, kg/m^3
μ_{matrix} – Dynamic viscosity of matrix fluid, Pa·S
μ_{CO_2} – Viscosity of CO_2, Pa·S
V – Volume of CO_2 bubble, m^3
$\frac{D}{Dt}$ – Material derivative of time
y – Depth, m
A – Correction factor, dimensionless
R_{CO_2} – Equivalent radius of CO_2, m
$\sum F$ – The sum of forces acting on CO_2, N
F_b – Buoyancy force, N
F_{st} –Surface force, N
F_d – Drag force, N
ϕ – Effective porosity of porous media, %
Re – Reynolds number
Ca – Capillary number
Bo – Bond number
Fr – Froude number
We – Weber number
θ – Contact angle, º
σ – Surface tension of CO_2-brine, N/m
R_p – Pore throat, m
d_p – Grain diameter of porous media, m
C_i – The aqueous concentrations of the volatile species, mole fractions
H_i – The Henry's law coefficients for each species *i*, MPa
P_y – The hydrostatic pressure at depth *y*, MPa
P_{st} – The surface tension pressure, MPa
γ – The viscosity coefficient used in Stokes Law, dimensionless

References

Bachu, S. (2008). "CO_2 storage in geological media: Role, means, status and barriers to deployment." Progress in Energy and Combustion Science **34**(2): 254-273.

Bando, S., F. Takemura, et al. (2004). "Viscosity of aqueous NaCl solutions with dissolved CO_2 at (30 to 60) ºC and (10 to 20) MPa." Journal of Chemical & Engineering Data **49**(5): 1328-1332.

Birkholzer, J. T. and Q. Zhou (2009). "Basin-scale hydrogeologic impacts of CO_2 storage: Capacity and regulatory implications." International Journal of Greenhouse Gas Control **3**(6): 745-756.

Chen, C. and D. Zhang (2010). "Pore-scale simulation of density-driven convection in fractured porous media during geological CO2 sequestration." Water Resour. Res. **46**(11): W11527.

Chen, Q., M. K. Gingras, et al. (2003). "A magnetic resonance study of pore filling processes during spontaneous imbibition in Berea sandstone." J. Chem. Phys. **119**: 9609.

Chiquet, P., J.-L. Daridon, et al. (2007). "CO2/water interfacial tensions under pressure and temperature conditions of CO2 geological storage." Energy Conversion and Management **48**(3): 736-744.

Cihan, A. and M. Y. Corapcioglu (2008). "Effect of compressibility on the rise velocity of an air bubble in porous media." Water Resour. Res. **44**(4): W04409.

Corapcioglu, M. Y., A. Cihan, et al. (2004). "Rise velocity of an air bubble in porous media: Theoretical studies." Water

Resour. Res. **40**(4): W04214.
Crandell, L. E., B. R. Ellis, et al. (2010). "Dissolution potential of SO2 co-injected with CO2 in geologic sequestration." Environmental Science and Technology **44**(1): 349-355.
Eccles, J. K., L. Pratson, et al. (2009). "Physical and economic potential of geological CO_2 storage in saline aquifers." Environmental Science & Technology **43**(6): 1962-1969.
Ergun, S. (1952). "Mass-Transfer Rate in Packed Columns."
Espinoza, D. N. and J. C. Santamarina (2010). "Water-CO2-mineral systems: interfacial tension, contact angle, and diffusion-Implications to CO2 geological storage." Water Resour. Res. **46**.
Glover and Walker (2011). "Grain-size to effective pore-size transformation derived from electrokinetic theory." Geophysics **76**(4).
Kneafsey, T. J. and K. Pruess (2010). "Laboratory flow experiments for visualizing carbon dioxide-induced, density-driven brine convection." Transport in Porous Media **82**(1): 123-139.
Kumagai, A. and C. Yokoyama (1999). "Viscosities of Aqueous NaCl Solutions Containing CO2 at High Pressures." Journal of Chemical & Engineering Data **44**(2): 227-229.
Li, L., C. A. Peters, et al. (2006). "Upscaling geochemical reaction rates using pore-scale network modeling." Advances in Water Resources **29**(9): 1351-1370.
Mansoori, S. A., S. Iglauer, et al. (2009). "Measurements of Non-Wetting Phase Trapping Applied to Carbon Dioxide Storage." Energy Procedia **1**(1): 3173-3180.
McGinnis, D. F., J. Greinert, et al. (2006). "Fate of rising methane bubbles in stratified waters: How much methane reaches the atmosphere?" Journal of Geophysical Research - Oceans **111**: C09007.
Nordbotten, J. M., M. A. Celia, et al. (2004). "Semianalytical solution for CO_2 leakage through an abandoned well." Environmental Science & Technology **39**(2): 602-611.
Oldenburg, C., J. Lewicki, et al. (2010). "Origin of the patchy emission pattern at the ZERT CO_2 release test." Environmental Earth Sciences **60**(2): 241-250.
Oldenburg, C. M. (2007). Migration mechanisms and potential impacts of CO_2 leakage and seepage. Carbon Capture and Storage. Wilson and Gerard, Blackwell.
Oldenburg, C. M. and J. L. Lewicki (2006). "On leakage and seepage of CO_2 from geologic storage sites into surface water." Environmental Geology **50**(5): 691-705.
Padhy, G. S., C. Lemaire, et al. (2007). "Pore size distribution in multiscale porous media as revealed by DDIF–NMR, mercury porosimetry and statistical image analysis." Colloids and Surfaces A: Physicochemical and Engineering Aspects **300**(1-2): 222-234.
Patzek, T. W., D. B. Silin, et al. (2003). "On vertical diffusion of gases in a horizontal reservoir." Transport in Porous Media **51**(2): 141-156.
Peters, C. A. (2009). "Accessibilities of reactive minerals in consolidated sedimentary rock: An imaging study of three sandstones." Chemical Geology **265**(1-2): 198-208.
Poletto, M. and D. D. Joseph. (1995). "The effect of density and viscosity of a suspension." Journal of Rheology.
Pollak, M. F. and E. J. Wilson (2009). "Regulating Geologic Sequestration in the United States: Early Rules Take Divergent Approaches." Environmental Science & Technology **43**(9): 3035-3041.
Pruess, K. (2008). "Leakage of CO_2 from geologic storage: Role of secondary accumulation at shallow depth." International Journal of Greenhouse Gas Control **2**(1): 37-46.
Pruess, K. (2008). "On CO_2 fluid flow and heat transfer behavior in the subsurface, following leakage from a geologic storage reservoir." Environmental Geology **54**(8): 1677-1686.
Riaz, A. and H. A. Tchelepi (2008). "Dynamics of vertical displacement in porous media associated with CO_2 sequestration." SPE Journal **13**(3): 305-313.
Roosevelt, S. E. and M. Y. Corapcioglu (1998). "Air bubble migration in a granular porous medium: Experimental studies." Water Resour. Res. **34**(5): 1131-1142.
Song, Y.-Q. (2001). "Pore sizes and pore connectivity in rocks using the effect of internal field." Magnetic Resonance Imaging **19**(3-4): 417-421.
Soubiran, J. and J. D. Sherwood (2000). "Bubble motion in a potential flow within a Venturi." International Journal of Multiphase Flow **26**(11): 1771-1796.
Span, R., E. W. Lemmon, et al. (2000). "A reference equation of State for the thermodynamic properties of nitrogen for temperatures from 63.151 to 1000 K and pressures to 2200 MPa." Journal of Physical and Chemical Reference Data **29**(6): 1361-1433.
Wallis, G. B. (1969). One-dimensional two-phase flow. New York,, McGraw-Hill.
Wang, S. and A. Clarens (2011). "The effects of CO2-brine rheology on leakage processes in geologic carbon sequestration." Water Resour. Res. **In Review**.
Widjajakusuma, J., B. Biswal, et al. (1999). "Quantitative prediction of effective material properties of heterogeneous media." Computational Materials Science **16**(1-4): 70-75.
Wollenweber, J., S. Alles, et al. (2010). "Experimental investigation of the CO_2 sealing efficiency of caprocks." International Journal of Greenhouse Gas Control **4**(2): 231-241.

Zhang, J. and L.-S. Fan (2003). "On the rise velocity of an interactive bubble in liquids." Chemical Engineering Journal **92**(1-3): 169-176.

Zhang, Y., C. M. Oldenburg, et al. (2009). "Probability estimation of CO_2 leakage through faults at geologic carbon sequestration sites." Energy Procedia **1**(1): 41-46.